Quenching of Frictional Vibration of a Rotating Circular Plate by Dynamic Absorbers*

Atsuo SUEOKA**, Takahiro RYU**,
Masato FUJIYAMA*** and Yutaka YOSHITAKE****

This paper deals with the quenching of self-excited vibrations of a rotating circular plate subjected to a concentrated frictional force as a function of relative slip velocity exerted on its outer circumference by dynamic absorbers. Results obtained by the method of multiple scales and the shooting method showed that (1) dynamic absorbers tuned to the natural frequency of the vibration mode to be controlled and arranged at a certain angle related to the vibration mode are the most effective, (2) such mountings of not one but several dynamic absorbers for every possible occurring mode, enable us to quench self-excited vibrations perfectly, and (3) thus, the effective masses of the dynamic absorbers are on the order of 10^{-3} of the mass of the circular plate. The analytical results are confirmed by an experiment concentrating on the perfect quenching of frictional vibrations of the rotating disk.

Key Words: Frictional Vibration, Self-Excited Vibration, Vibration Control, Nonlinear Vibration, Damper, Rotating Disk, Method of Multiple Scales, Shooting Method

1. Introduction

As a series of studies on quenching self-excited vibrations such as squeals of disk brakes and of railway vehicle wheels rolling along a curved rail, the authors[1),(2)] and Harada *et al.*[3)] analyzed the effect of the imperfection existing in a rotating disk and considered the influence of the imperfection on the frictional vibration. On the other hand, some methods of vibration control using dynamic absorbers have been investigated for the forced vibration of a disk[4),(5)]. However, there are few investigations concerning the means of quenching self-excited vibrations of a rotating disk.

In this report, the authors present an effective method by which the self-excited vibration of disk rotating at a low speed can be perfectly controlled by dynamic absorbers attached to the disk without the effect of internal resonances. From theoretical and numerical analyses of the model described in the previous report[1)], it was made clear that the self-excited vibration could be effectively and perfectly quenched by arranging a few dynamic absorbers on the disk. Furthermore, a good qualitative agreement between the results of theoretical analysis for the perfect quenching of self-excited vibration and the experimental ones was confirmed.

2. Theoretical Analysis

The boundary condition of the disk for the inner circumference ($r=r_0$) is fixed, and that for the outer circumference ($r=R$) is free, as shown in Fig. 1, where (r, θ) is the fixed coordinate system in space. The disk rotates at an angular velocity ω, and an axial frictional force $\bar{P}$ acts at a point $(R, 0)$ on its outer circumference through a rigid friction rod subjected to a normal load P. N dynamic absorbers are mounted at the points (r_n, ϕ_n) in the fixed coordinate system (r, ϕ) on the disk. The mass, viscous damping

* Received 7th March, 1994. Japanese original: Trans. Jpn. Soc. Mech. Eng., Vol. 59, No. 561, C (1993), pp. 1335-1342. (Received 22nd October, 1992)
** Faculty of Engineering, Kyushu University 36, 6-10-1 Hakozaki, Higashi-ku, Fukuoka 812, Japan
*** Toyota Motor Corporation, 1 Toyota-cho, Toyota 471, Japan
**** Faculty of Engineering, Nagasaki University, 1-14 Bunkyo-cho, Nagasaki 852, Japan

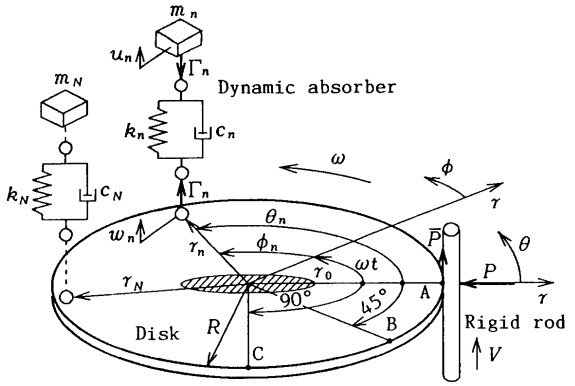

Fig. 1 Analytical model and coordinate system of a disk

coefficient and spring constant of every dynamic absorber are m_n, c_n and k_n, respectively (see Fig. 1), where $n=1, \cdots, N$. This paper deals with the fundamental theoretical analysis of the self-excited vibrations of the disk without the effect of internal resonances. In order to enable us to also develop the theoretical treatment for the disk with the effect of internal resonances, the disk is regarded as a Mindlin circular plate.

In this study, since the rotating speed is much lower than the natural frequencies of the circular plate, the centrifugal force and the Coriolis force are neglected. The equations of motion of the disk are represented by the following equations, in which the fixed coordinate system (r, θ) is used:

$$\left.\begin{aligned}
&\frac{\partial M_r}{\partial r}+\frac{1}{r}\frac{\partial M_{r\theta}}{\partial \theta}+\frac{M_r-M_\theta}{r}-Q_r \\
&\quad=\frac{\rho H^3}{12}\left(\frac{\partial}{\partial t}+\omega\frac{\partial}{\partial \theta}\right)^2\psi_r \\
&\frac{\partial M_{r\theta}}{\partial r}+\frac{1}{r}\frac{\partial M_\theta}{\partial \theta}+\frac{2M_{r\theta}}{r}-Q_\theta \\
&\quad=\frac{\rho H^3}{12}\left(\frac{\partial}{\partial t}+\omega\frac{\partial}{\partial \theta}\right)^2\psi_\theta \\
&\frac{\partial Q_r}{\partial r}+\frac{1}{r}\frac{\partial Q_\theta}{\partial \theta}+\frac{Q_r}{r} \\
&\quad=\rho H\left(\frac{\partial}{\partial t}+\omega\frac{\partial}{\partial \theta}\right)^2 w-\frac{\bar{P}}{r}\delta(r-R)\delta(\theta) \\
&\quad-\sum_{n=1}^{N}\Gamma_n(t)\delta(r-r_n)\delta(\theta-\theta_n)/r
\end{aligned}\right\} \quad (1)$$

where M_r, $M_{r\theta}$ and M_θ are moments, Q_r and Q_θ are shearing forces, w, ψ_r and ψ_θ are an axial displacement and angular displacements, respectively, H is the thickness of the disk, t is time, ρ is density, $\delta(\cdot)$ is the Dirac delta function, and $\Gamma_n(t)$ is the contact force between the n-th dynamic absorber and the disk. The disk is axisymmetrical and has a few steps as shown in Fig. 2. However, the subscripts referring to the ring number are omitted here.

The equation of motion of the n-th dynamic absorber and the contact force $\Gamma_n(t)$ are given as

$$\ddot{u}_n+2\zeta_n\omega_n(\dot{u}_n-\dot{w}_n)+\omega_n^2(u_n-w_n)=0 \quad (2)$$

$$\Gamma_n(t)=m_n\{2\zeta_n\omega_n(\dot{u}_n-\dot{w}_n)+\omega_n^2(u_n-w_n)\} \quad (3)$$

where $\zeta_n=c_n/2\sqrt{m_nk_n}$, $\omega_n=\sqrt{k_n/m_n}$, u_n is the displacement of the n-th dynamic absorber, and $w_n=w(r_n, \theta_n)$ is the displacement of the disk at the location to which the n-th dynamic absorber is attached.

We assume the displacements of the disk at a point (r, θ), which is fixed in space, as

$$\left.\begin{aligned}
\psi_r&=\sum_{ms}\bar{\psi}_{r,ms}(C_{ms}\cos m\theta+D_{ms}\sin m\theta) \\
\psi_\theta&=\sum_{ms}\bar{\psi}_{\theta,ms}(C_{ms}\sin m\theta-D_{ms}\cos m\theta) \\
w&=\sum_{ms}\bar{w}_{ms}(C_{ms}\cos m\theta+D_{ms}\sin m\theta)
\end{aligned}\right\} \quad (4)$$

where m and s are the numbers of nodal diameters and nodal circles $(m, s=0, 1, \cdots)$, the symbol $\sum_{ms}$ means a double summation from zero to ∞, with respect to the subscripts m and s, and C_{ms} and D_{ms} are both unknown functions of time. $\bar{w}_{ms}$, $\bar{\psi}_{r,ms}$, and $\bar{\psi}_{\theta,ms}$ are the characteristic functions of radial coordinate r of w, ψ_r and ψ_θ for the (m, s)-mode corresponding to natural circular frequency ω_{ms}, and the shape functions satisfy the normalized relation[6].

Substituting Eq. (4) into Eq. (1) and applying the orthogonal relation, the relationships between natural frequencies and the characteristic functions and the stress-displacement relations, we obtain the following equations[1),6]:

$$\begin{aligned}
&\ddot{C}_{ms}+2m\omega\dot{D}_{ms}+2\zeta_{ms}\omega_{ms}(\dot{C}_{ms}+m\omega D_{ms}) \\
&\quad+(\omega_{ms}^2-m^2\omega^2)C_{ms} \\
&\quad=\varkappa_{ms}\bar{P}+\sum_n\varkappa_{ms}^n\Gamma_n(t)\cos m\theta_n \quad (5.\text{a}) \\
&\dot{D}_{ms}-2m\omega\dot{C}_{ms}+2\zeta_{ms}\omega_{ms}(\dot{D}_{ms}-m\omega C_{ms}) \\
&\quad+(\omega_{ms}^2-m^2\omega^2)D_{ms}=\sum_n\varkappa_{ms}^n\Gamma_n(t)\sin m\theta_n \quad (5.\text{b})
\end{aligned}$$

where $\sum_n$ indicates summation from 1 to N, with respect to n, and

$$\varkappa_{ms}=\bar{w}_{ms}(R)/\rho R^5,\ \varkappa_{ms}^n=\bar{w}_{ms}(r_n)/\rho R^5,$$
$$\theta_n=\omega t+\phi_n. \quad (6)$$

In addition, the modal damping ratios are introduced in Eq. (5), and the modal damping ratio for the (m, s)-mode is represented by ζ_{ms}.

The relationship between friction force $\bar{P}$ and normal load P acting on the rigid friction rod, and the relative slip velocity v between disk and friction rod are expressed as follows:

$$\left.\begin{aligned}
\bar{P}&=P\cdot f(v) \\
f(v)&=e_1v^3-e_2v+e_3
\end{aligned}\right\} \quad (7)$$

$$v=V-(\partial/\partial t+\omega\partial/\partial\theta)w|_{r=R,\,\theta=0} \quad (8)$$

where $f(v)$ is the coefficient of friction defined by a polynomial expression of the third order with respect to v, e_1, e_2 and e_3 are suitable constants, and V is the sweep velocity of a friction rod in the axial direction.

Now, we introduce a small parameter ε. The rotating speed ω, the viscous damping ratios ζ_{ms}, the frictional force $\bar{P}$ and the contact forces $\Gamma_n(t)$ are small and it is assumed that they are all of order ε. Then, substituting Eqs. (3) and (7) into Eq. (5),

and taking the terms up to the first order in ε into account, we obtain the following equations:

$$\ddot{c}_{ms}+\omega_{ms}^2 c_{ms}=\varepsilon[-2\zeta_{ms}\omega_{ms}\dot{c}_{ms} -2m\omega\dot{d}_{ms}+K_{ms}^P\{f(v)-f(V)\} +\sum_n \varkappa_{ms}^n \Gamma_n(t)\cos m(\omega t+\phi_n)] \quad (9.a)$$

$$\ddot{d}_{ms}+\omega_{ms}^2 d_{ms}=\varepsilon[-2\zeta_{ms}\omega_{ms}\dot{d}_{ms} +2m\omega\dot{c}_{ms}+\sum_n \varkappa_{ms}^n \Gamma_n(t)\sin m(\omega t+\phi_n)] \quad (9.b)$$

where $K_{ms}^P=\varkappa_{ms}P$, and c_{ms} and d_{ms} are the fluctuating components of C_{ms} and D_{ms}, respectively, satisfying the following relations.

$$C_{ms}=C_{ms}^0+c_{ms},\ D_{ms}=D_{ms}^0+d_{ms}$$
$$C_{ms}^0=\varepsilon K_{ms}^P f(V)/\omega_{ms}^2,\ D_{ms}^0=0 \quad (10)$$

In Eq. (9), the higher-frequency components of ω_{ms} and the lower-frequency ones of $m\omega$ coexist. The method of multiple scales[7] which is very effective for such a system is applied here to obtain the approximate solutions of the first order to Eqs. (2) and (9). In what follows, we describe only the expressions which are necessary for the approximate solutions of the first order.

First, we introduce new independent variables $T_i=\varepsilon^i t$, where $i=0$ and 1. Then, we obtain

$$d/dt=D_0+\varepsilon D_1,\ d^2/dt^2=D_0^2+2\varepsilon D_0 D_1 \quad (11)$$

where $D_0=\partial/\partial T_0$ and $D_1=\partial/\partial T_1$.

The solutions of Eq. (9) are assumed as

$$c_{ms}(t,\varepsilon)=c_{ms}^1(T_0,T_1)+\varepsilon c_{ms}^2(T_0,T_1)$$
$$d_{ms}(t,\varepsilon)=d_{ms}^1(T_0,T_1)+\varepsilon d_{ms}^2(T_0,T_1) \quad (12)$$
$$u_n(t,\varepsilon)=u_n^1(T_0,T_1)+\varepsilon u_n^2(T_0,T_1).$$

Substituting Eq. (11) into Eqs. (2) and (9), and equating coefficients of like powers of ε, we obtain, from the comparison of the coefficients of ε^0,

$$D_0^2 c_{ms}^1+\omega_{ms}^2 c_{ms}^1=0 \quad (13.a)$$
$$D_0^2 d_{ms}^1+\omega_{ms}^2 d_{ms}^1=0 \quad (13.b)$$
$$D_0^2 u_n^1+2\zeta_n\omega_n D_0 u_n^1+\omega_n^2 u_n^1 =\sum_{kl}\bar{w}_{kl}(r_n)\{\omega_n^2(c_{kl}^1\cos k\theta_n^1+d_{kl}^1\sin k\theta_n^1) +2\zeta_n\omega_n(D_0 c_{kl}^1\cos k\theta_n^1+D_0 d_{kl}^1\sin k\theta_n^1)\}. \quad (13.c)$$

Next, from the comparison of the coefficients of ε^1, we obtain

$$D_0^2 c_{ms}^2+\omega_{ms}^2 c_{ms}^2= -2D_0D_1c_{ms}^1-2\zeta_{ms}\omega_{ms}D_0c_{ms}^1-2m\omega D_0 d_{ms}^1 +K_{ms}^P e_1[-3V^2\sum_{kl}\bar{w}_{kl}(R)D_0c_{kl}^1 +3V\{\sum_{kl}\bar{w}_{kl}(R)D_0c_{kl}^1\}^2-\{\sum_{kl}\bar{w}_{kl}(R)D_0c_{kl}^1\}^3] +K_{ms}^P e_2\sum_{kl}\bar{w}_{kl}(R)D_0c_{kl}^1 +\sum_n\varkappa_{ms}^n m_n[\omega_n^2\{u_n^1-\sum_{kl}\bar{w}_{kl}(r_n)(c_{kl}^1\cos k\theta_n^1 +d_{kl}^1\sin k\theta_n^1)\} +2\zeta_n\omega_n\{D_0u_n^1-\sum_{kl}\bar{w}_{kl}(r_n)(D_0c_{kl}^1\cos k\theta_n^1 +D_0d_{kl}^1\sin k\theta_n^1)\}]\cos m\theta_n^1 \quad (14.a)$$

$$D_0^2 d_{ms}^2+\omega_{ms}^2 d_{ms}^2= -2D_0D_1d_{ms}^1-2\zeta_{ms}\omega_{ms}D_0d_{ms}^1+2m\omega D_0c_{ms}^1 +\sum_n\varkappa_{ms}^n m_n[\omega_n^2\{u_n^1-\sum_{kl}\bar{w}_{kl}(r_n)(c_{kl}^1\cos k\theta_n^1 +d_{kl}^1\sin k\theta_n^1)\} +2\zeta_n\omega_n\{D_0u_n^1-\sum_{kl}\bar{w}_{kl}(r_n)(D_0c_{kl}^1\cos k\theta_n^1 +D_0d_{kl}^1\sin k\theta_n^1)\}]\sin m\theta_n^1 \quad (14.b)$$

$$D_0^2 u_n^2+2\zeta_n\omega_n D_0 u_n^2+\omega_n^2 u_n^2 =\omega_n^2\sum_{kl}\bar{w}_{kl}(r_n)(c_{kl}^2\cos k\theta_n^1+d_{kl}^2\sin k\theta_n^1) -2\zeta_n\omega_n[D_1u_n^1 -\sum_{kl}\bar{w}_{kl}(r_n)\{(D_1c_{kl}^1+D_0c_{kl}^2)\cos k\theta_n^1 +(D_1d_{kl}^1+D_0d_{kl}^2)\sin k\theta_n^1\}]-2D_0D_1u_n^1 \quad (14.c)$$

where $\theta_n^1=\omega T_1+\phi_n$.

The solutions of Eq. (13) are written as

$$c_{ms}^1=A_{ms}(T_1)\exp(j\omega_{ms}T_0)+cc$$
$$d_{ms}^1=B_{ms}(T_1)\exp(j\omega_{ms}T_0)+cc$$
$$u_n^1=\sum_{kl}U_{kl}^n(T_1)\exp(j\omega_{kl}T_0)+cc$$
$$U_{kl}^n=\frac{\omega_n^2(\omega_n^2+4\zeta_n^2\omega_{kl}^2-\omega_{kl}^2)-2j\zeta_n\omega_n\omega_{kl}^3}{(\omega_n^2-\omega_{kl}^2)^2+4\zeta_n^2\omega_n^2\omega_{kl}^2} \times\bar{w}_{kl}(r_n)(A_{kl}\cos k\theta_n^1+B_{kl}\sin k\theta_n^1) \quad (15)$$

where cc stands for the complex conjugate of preceding terms, and $j^2=-1$.

Substituting Eq. (14) into the right-hand side of Eqs. (13.a) and (13.b), and eliminating the secular terms yields

$$-j[2\omega_{ms}D_1A_{ms}+2\zeta_{ms}\omega_{ms}^2A_{ms}+2m\omega\omega_{ms}B_{ms} +K_{ms}^P(3e_1V^2-e_2)\bar{w}_{ms}(R)\omega_{ms}A_{ms} +3K_{ms}^Pe_1\bar{w}_{ms}(R)\omega_{ms}A_{ms}[\{\bar{w}_{ms}(R)\}^2\omega_{ms}^2A_{ms}\bar{A}_{ms} +2\sum_{kl}'\{\bar{w}_{kl}(R)\}^2\omega_{kl}^2A_{kl}\bar{A}_{kl}]]+\sum_n\varkappa_{ms}^n m_n[\omega_n^2\{U_{ms}^n -\bar{w}_{ms}(r_n)(A_{ms}\cos m\theta_n^1+B_{ms}\sin m\theta_n^1)\} +2j\zeta_n\omega_n\omega_{ms}\{U_{ms}^n-\bar{w}_{ms}(r_n)(A_{ms}\cos m\theta_n^1 +B_{ms}\sin m\theta_n^1)\}]\cos m\theta_n^1=0 \quad (16.a)$$

$$-j(2\omega_{ms}D_1B_{ms}+2\zeta_{ms}\omega_{ms}^2B_{ms} -2m\omega\omega_{ms}A_{ms})+\sum_n\varkappa_{ms}^n m_n[\omega_n^2\{U_{ms}^n -\bar{w}_{ms}(r_n)(A_{ms}\cos m\theta_n^1+B_{ms}\sin m\theta_n^1)\} +2j\zeta_n\omega_n\omega_{ms}\{U_{ms}^n-\bar{w}_{ms}(r_n)(A_{ms}\cos m\theta_n^1 +B_{ms}\sin m\theta_n^1)\}]\sin m\theta_n^1=0 \quad (16.b)$$

where the symbol $\sum_{kl}'$ means a double summation from zero to ∞ with respect to the subscripts k and l for $(k,l)\neq(m,s)$, and $\bar{A}_{ms}$ are $\bar{B}_{ms}$ are the complex conjugate of A_{ms} and B_{ms}, respectively. We write A_{ms} and B_{ms} in Eq. (16) in the following form:

$$A_{ms}=x_{ms}\exp(j\alpha_{ms})/2$$
$$B_{ms}=y_{ms}\exp(j\beta_{ms})/2 \quad (17)$$
$$\Theta_{ms}=\alpha_{ms}-\beta_{ms}$$

where x_{ms}, y_{ms}, α_{ms} and β_{ms} are all real functions of T_1.

Substituting Eq. (17) into Eq. (16), and separating real and imaginary parts, we obtain the following simultaneous ordinary differential equations:

$$a_{ms}'=-\zeta_{ms}\omega_{ms}a_{ms}-m\omega b_{ms}\cos\Theta_{ms} +K_{ms}^P\{(e_2-3e_1V^2)X_{ms} -3e_1X_{ms}(X_{ms}^2+2\sum_{kl}'X_{kl}^2)/4\}/2 -(\omega_{ms}b_{ms}\sin\Theta_{ms}/4)\sum_nK_{ms}^nY_{ms}^n\sin 2m\theta_n^1 -\omega_{ms}\sum_nK_{ms}^nZ_{ms}^n\{a_{ms}(1+\cos 2m\theta_n^1) +b_{ms}\sin 2m\theta_n^1\cos\Theta_{ms}\}/4 \quad (18.a)$$

$$b_{ms}'=-\zeta_{ms}\omega_{ms}b_{ms}+m\omega a_{ms}\cos\Theta_{ms} +(\omega_{ms}a_{ms}\sin\Theta_{ms}/4)\sum_nK_{ms}^nY_{ms}^n\sin 2m\theta_n^1 -\omega_{ms}\sum_nK_{ms}^nZ_{ms}^n\{a_{ms}\sin 2m\theta_n^1\cos\Theta_{ms} +b_{ms}(1-\cos 2m\theta_n^1)\}/4 \quad (18.b)$$

$$\Theta_{ms}'=(b_{ms}/a_{ms}-a_{ms}/b_{ms})\{m\omega\sin\Theta_{ms} -(\omega_{ms}\cos\Theta_{ms}/4)\sum_nK_{ms}^nY_{ms}^n\sin 2m\theta_n^1\} -(\omega_{ms}/2)\sum_nK_{ms}^nY_{ms}^n\cos 2m\theta_n^1$$

$$+(b_{ms}/a_{ms}+a_{ms}/b_{ms})(\omega_{ms}\sin\Theta_{ms} \times\sum_n K^n_{ms}Z^n_{ms}\sin 2m\theta^1_n)/4 \quad (18.c)$$

where the notation "′" indicates the derivative with respect to T_1,

$$a_{ms}=\omega_{ms}x_{ms},\ b_{ms}=\omega_{ms}y_{ms}$$
$$K^n_{ms}=\{\bar{w}_{ms}(r_n)\}^2/\rho R^5,\ X_{ms}=\bar{w}_{ms}(R)a_{ms}$$
$$Y^n_{ms}=\frac{m_n(1-\Omega^{n2}_{ms}+4\zeta^2_n\Omega^{n2}_{ms})}{(1-\Omega^{n2}_{ms})^2+4\zeta^2_n\Omega^{n2}_{ms}}$$
$$Z^n_{ms}=\frac{2m_n\zeta_n\Omega^{n3}_{ms}}{(1-\Omega^{n2}_{ms})^2+4\zeta^2_n\Omega^{n2}_{ms}}$$

and $\Omega^n_{ms}=\omega_{ms}/\omega_n$. a_{ms} and b_{ms} represent the velocity amplitudes of c_{ms} and d_{ms}, respectively.

3. Numerical Computational Results

3.1 Computational model and calculation method

In Fig. 2 are shown the dimensions of the circular steel plate used in the analysis in this report. The theoretical natural frequencies and the experimental modal damping ratios[8] for several modes of the circular plate are indicated in Table 1. In the following numerical computation, we assume that normal load $P=19.6$ N, rotational speed $\Omega=\omega/2\pi=0.05$ Hz, sweep velocity of the friction rod in the axial direction $V=0.12$ m/s, and that the dynamic absorbers are all located on the outer circumference of the circular plate. Furthermore, the characteristic of friction is assumed as follows: $e_1=25\ s^3/m^3$, $e_2=2.0$ s/m and $e_3=0.45$.

The damping ratio ζ_n of the dynamic absorbers was measured by exciting them by an electrodynamic excitor. In the experiment without dynamic absorbers, we confirmed only the self-excited vibrations of the (2, 0) single mode, in which the number of nodal diameters $m=2$, and that of nodal circles $s=0$, and the (3, 0) single mode as mentioned below. The damping ratios of the dynamic absorbers for controlling the (2, 0)- and the (3, 0)-modes were experimentally set at 0.054 and 0.092, respectively. In this study, thus, we chose the dynamic absorbers with light damping as the subject of numerical computation and experiment.

Table 1 Natural frequencies of a circular plate (Hz) and damping ratios

Mode (m,s)	(1,0)	(0,0)	(2,0)	(3,0)	(4,0)
$\omega_{ms}/2\pi$	355	429	643	1549	2861
ζ_{ms}	15.2×10^{-3}	8.08	1.70	0.78	6.13

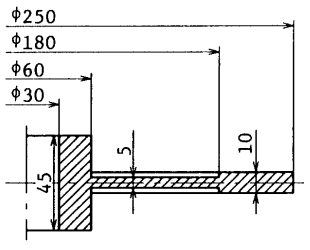

Fig. 2 Dimensions of a circular plate (Unit: mm)

Because of the imperfection due to dynamic absorbers, the periodically fluctuating terms such as $\sin 2m(\omega T_1+\phi_n)$ and $\cos 2m(\omega T_1+\phi_n)$ appear in Eq. (18), and thus Eq. (18) has a periodic solution accompanied by periodic fluctuation. We applied the shooting method[6] to the solution for this periodic vibration. The method uses both the Runge-Kutta-Gill method and Newton-Raphson method in combination, and can extract the periodic solution efficiently.

First, the direct numerical integral method was applied to the simultaneous ordinary differential equations of Eqs. (5) and (18), taking the five modes indicated in Table 1 into account. The results showed that only the self-excited vibrations composed of the (2, 0) and the (3, 0) single modes were generated for the parameters used here. Thus, the amplitudes of the other modes which did not occur were equal to zero in these vibrations. As these amplitudes of the other modes appear in the denominators of Eq. (18.c), an approach such as the shooting method in which the Jacobian matrix is used cannot be applied to Eq. (18). Therefore, the periodic solutions and their stabilities are determined as follows.

(1) By applying the shooting method to the simultaneous ordinary differential equations with respect to the (m, s) single mode extracted from Eq. (18), we obtain the periodic solution with period $\pi/m\omega$.

(2) The stability of the solution should be judged with full consideration of the relationship between the corresponding mode and the other modes. We integrate Eq. (18) over great many periods, with the initial values which lead to periodic solution obtained above for the (m, s)-mode and with the very small initial values of the variables a_{kl}, b_{kl} and Θ_{kl} for other (k, l)-modes.

(3) From the result of integration, if the values corresponding to the (m, s)-mode remain near the initial values and the other values tend to zero, the periodic solution obtained in (1) mentioned above is stable, otherwise it is unstable.

(4) Substituting the periodic solution of Eq. (18) obtained in (1) to (3) above into Eqs. (15), (10) and (4), we obtain the waveform of the self-excited vibration of the rotating disk having dynamic absorbers represented by the fixed coordinates in space. The waveform shows a beat phenomenon.

3.2 Numerical computational results and discussion

Figure 3 shows the numerical computational

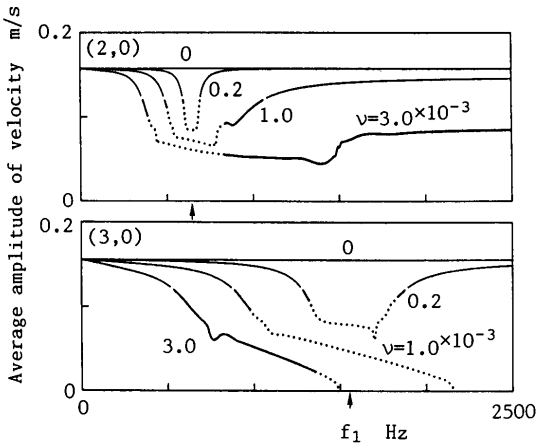

Fig. 3 Control effect of self-excited vibration exerted by a dynamic absorber

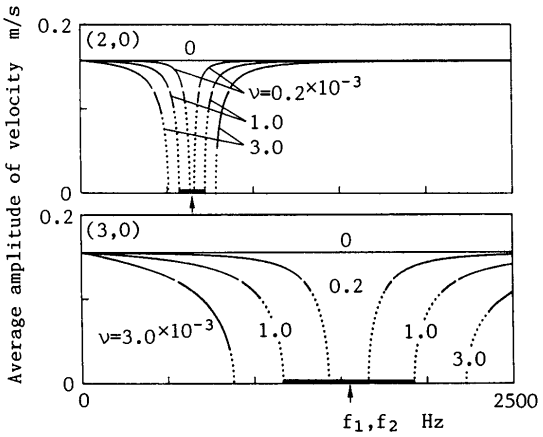

Fig. 4 Control effect of self-excited vibration exerted by two dynamic absorbers

result of the (2, 0)- and (3, 0)-modes with parameter ν ($=m_1/M$) of mass ratio of dynamic absorber to disk when only one dynamic absorber is mounted on the disk ($N=1$). The abscissa is the natural frequency of the dynamic absorber $f_1=\omega_1/2\pi$ [Hz]. In the case that the dynamic absorber is attached to the disk, the vibration of the disk shows the beat phenomenon because of the imperfection due to the dynamic absorber. Therefore, the ordinate is the average amplitude of velocity of the (2, 0)- and (3, 0)-modes calculated from the average values of a_{ms} and b_{ms}. The bold and the fine lines indicate the solutions for which the relative velocities between disk and rigid friction rod are positive and negative, respectively, when computed from the average velocity amplitudes. The solid and the dotted lines show the stable and the unstable solutions, respectively. The solutions with negative relative velocity may correspond to the self-excited vibration of stick-slip type. Comparing the case having absorber with that having no absorber ($\nu=0$) in Fig. 3, the average velocity amplitudes are decreased when the natural frequency of the dynamic absorber is tuned to that of the disk (see arrows in the figures), and so the absorber certainly suppresses the self-excited vibration. However, the solution for the (2, 0)-mode exists, though it is unstable. This is because the (3, 0)-mode is dominant and stable when the dynamic absorber is set to control the self-excited vibration of the (2, 0)-mode. Therefore, the (2, 0)-mode can be generated, if the stable (3, 0)-mode is perfectly controlled by some means. Hence, it is impossible to perfectly control the self-excited vibration using only one dynamic absorber and for the mass ratio of dynamic absorber to disk indicated in the figure. In the case that the mass of the dynamic absorber is large, there is a region with no finite amplitude for the (3, 0)-mode, that is, one in which the vibration is perfectly controlled. This shows that it is easy to quench the (3, 0)-mode, compared with the (2, 0)-mode.

Figure 4 shows the result similar to Fig. 3 for two dynamic absorbers ($N=2$), where the natural frequencies of the absorbers are equal to each other ($f_1=f_2$), and are variable. In order to clarify the effect of two dynamic absorbers, we use the mass ratio ν [$=(m_1+m_2)/M$] of all absorbers to the disk as a parameter. The upper and the lower figures correspond to the arrangements of the absorbers at an angle of 45° for the (2, 0)-mode and at an angle of 30° for the (3, 0)-mode, respectively. Moreover, the positions of the arrow in the figures show the natural frequencies of the two modes to be controlled. For example, in the case of $\nu=1.0\times10^{-3}$, the self-excited vibration can be perfectly quenched by tuning the natural frequency of the dynamic absorbers to a frequency in the range drawn with a thick line on the abscissa (called the perfect quenching region). Therefore, in order to perfectly quench the self-excited vibration by arranging the dynamic absorbers on the disk, it is very effective to arrange more than two dynamic absorbers tuned to a frequency in the perfect quenching region at a particular angle. The consideration of the angle will be mentioned below. Additionally, we can quench the self-excited vibrations of the disk perfectly even if the mass ratio of all dynamic absorbers to the disk is on the order of 10^{-3}. On the basis of the results mentioned above, we used two dynamic absorbers in the numerical computation and the experiment in the following.

Figure 5(a) shows the influence of the opening angle $\Delta\phi_{20}$ upon the quenching of the self-excited vibration where two dynamic absorbers with masses $m_1=m_2=2$g tuned to the natural frequency of 1549 Hz of the (3, 0)-mode (whose positions are illustrated in

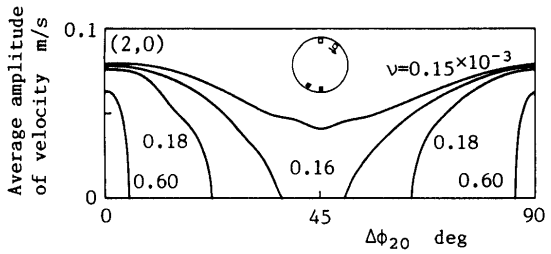

(a) For the (2, 0)-mode

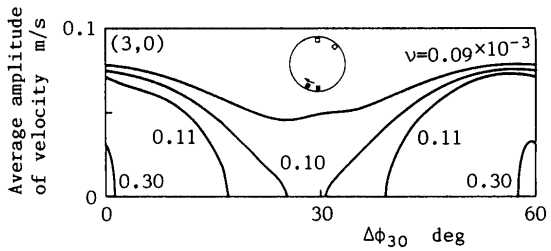

(b) For the (3, 0)-mode

Fig. 5 Effect of opening angle between dynamic absorbers

Fig. 5 with the symbols ■, and which are called dynamic absorbers for the (3, 0)-mode) are installed at an opening angle of $\Delta\phi_{30}=30°$, and two dynamic absorbers tuned to the natural frequency of 643 Hz of the (2, 0)-mode (whose positions are illustrated in Fig. 5 with the symbols □, and which are called dynamic absorbers for the (2, 0)-mode) are also mounted. Similarly, Fig. 5(b) shows the influence of the opening angle $\Delta\phi_{30}$ upon the quenching of the self-excited vibration where two dynamic absorbers with masses $m_1=m_2=2$g for the (2, 0)-mode are installed at an opening angle of $\Delta\phi_{20}=45°$, and two dynamic absorbers for the (3, 0)-mode are also mounted. In Figs. 5(a) and 5 (b), we can see respectively the states in which only the (2, 0)-mode can occur under the condition of perfect quenching of the (3, 0)-mode and only the (3, 0)-mode can occur under the condition of perfect quenching of the (2, 0)-mode. The parameter ν in the figures is the mass ratio of the two dynamic absorbers whose opening angle is changed, to the disk. From the figures, for the case that the dynamic absorbers are perfectly tuned to the mode to be controlled, the opening angles near $\Delta\phi_{20}=45°$ and near $\Delta\phi_{30}=30°$ are the most effective for the (2, 0)- and the (3, 0)-modes, respectively. That is, the perfect quenching regions are effectively utilized by arranging the dynamic absorbers at an angle corresponding to the interval between loop and node of the mode to be controlled. Here, the solutions in Fig. 5 are all stable ones with positive relative velocity.

Figure 6 shows the tolerable quantity of the detuning for the (2, 0)- and (3, 0)-modes, that is, the

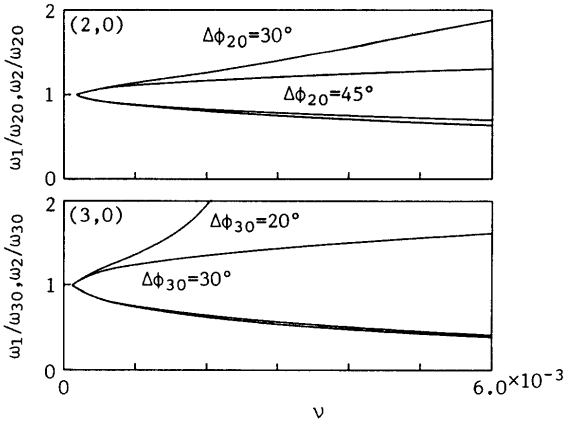

Fig. 6 Perfect quenching regions of self-excited vibration

perfect quenching region for the case of two dynamic absorbers. The abscissa represents ν, and the ordinate the natural frequency ratios of two dynamic absorbers to the (2, 0)- and (3, 0)-modes. The parameter in both figures is the opening angle between the dynamic absorbers. Perfect quenching is possible by tuning the natural frequency of the dynamic absorbers to the inside of the C-shaped region in the figures. From the figures, where the dynamic absorbers are installed at an angle of 45° for the (2, 0)-mode, perfect quenching is possible in the region of $\omega_1/\omega_{20}=\omega_2/\omega_{30}=0.88\sim1.12$ even for ν on the order of 10^{-3}, which shows a fairly robust characteristic. As the detuning of the dynamic absorbers is increased, the perfect quenching regions become wider at opening angles of 30° for the (2, 0)-mode and of 20° for the (3, 0)-mode.

4. Experimental Results

4.1 Experimental apparatus and experimental approach

A photograph of the experimental apparatus is shown in Fig. 7. The material of the disk was SK 4, and the dimensions were the same as those shown in Fig. 2. The inner circumference was fixed by the M 30 nut, and the disk was driven at a speed of $\Omega=0.05$ Hz by a motor. The frictional rod, which was 20 mm in diameter and 1.2 m in length, was made of S 45 C. Both ends of the friction rod were fixed to the acrylic plates through rubber in parallel with the guide bar so that no natural frequencies of the friction rod coincided with those of the disk. The normal load of 19.6 N was applied to the friction rod by a load adjuster with a spring through the bearings on the outer circumference of the disk, and the friction rod was swept by another motor. To set the relative velocity V in the axial direction at 0.12 m/s and in the circumferential direction at zero, the sweep velocity and the sweep

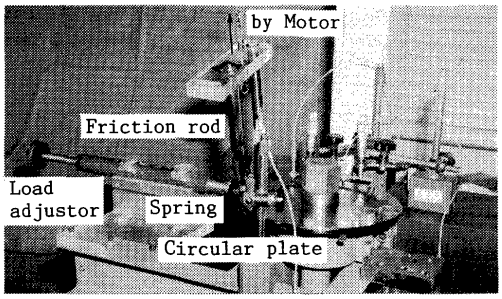

Fig. 7 Outline of experimental apparatus

angle of the rod were changed, according to the rotating speed of the circular plate. The frictional surface was finished with emery paper of #800, and was ultrasonically cleaned before the experiment. During the experiment, the steady-state condition of the friction surface was maintained by wiping with a cloth containing acetone. The squeal produced by contact between the circular plate and the friction rod was always detected electrically in the experiment.

The displacements of the vibration were measured by eddy-current displacement meters having no contact with the circular plate, and the arrangement is shown in Fig. 1. In the figure, point A is a frictional point, and the vibration was measured at points A and B for the (2, 0)-mode and at points A and C for the (3, 0)-mode so that the measuring points correspond to the loop and the node of the characteristic mode of the circular plate in the stationary state.

The dynamic absorbers were composed of small metal masses and rubber. The natural frequency of each dynamic absorber was tuned, by means of an excitation experiment using an electrodynamic excitor, to that of the mode to be controlled as accurately as possible, and each absorber was set near the outer circumference of the circular plate.

4.2 Experimental results and discussion

In Figs. 8(a) and 8(c), the waveforms with time of the (2, 0)- and the (3, 0)-modes are indicated for the case where no dynamic absorbers are installed. Here, the time axis is reduced. We call the waveforms envelope waveforms in the following. The vibration waveforms of every mode and the results of the frequency analysis are also indicated in Figs. 8(b) and 8(d). The abscissa in Figs. 8(a) and 8(c) represents real time and the ordinate the displacement, and the points S and E in the figures show the starting time and the finishing time for sweeping the friction rod. From the figures, because of rotation of the circular plate, the amplitudes at the points B and C for the (2, 0)- and the (3, 0)-modes do not vanish, and the vibration mode deviates only a little in the rotating direction. We can also see weak beats in the

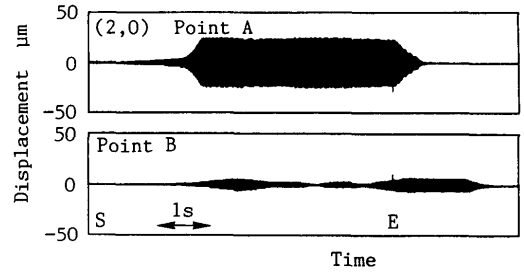

(a) Envelope waveforms of the (2, 0)-mode

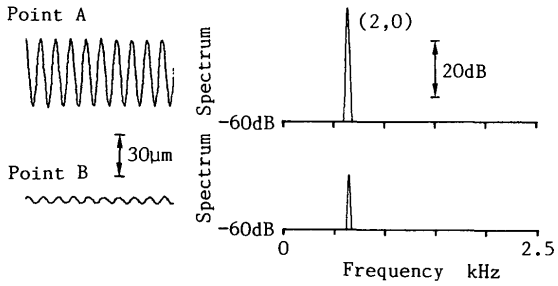

(b) Vibration waveforms of the (2, 0)-mode and frequency analyses

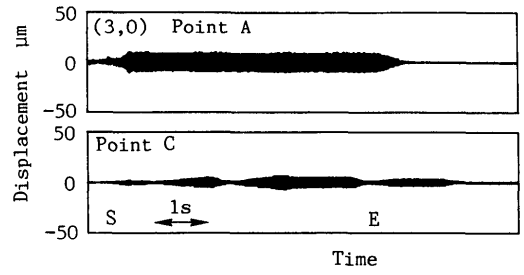

(c) Envelope waveforms of the (3, 0)-mode

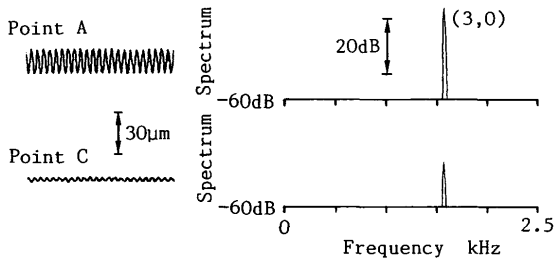

(d) Vibration waveforms of the (3, 0)-mode and frequency analyses

Fig. 8 Vibration of disk without dynamic absorbers

(2, 0)- and the (3, 0)-modes. This is because the circular plate possesses slight imperfection due to errors in making and setting it. From the measured result of the dimensions of the circular plate and the numerical computational result for the case that the imperfection is added to the circular plate, it was clarified that the imperfection was very small, compared with the mass of the circular plate.

Moreover, imperfection of this degree had little effect upon the quenching of the self-excited vibration from the numerical computation.

For this circular plate, it was clarified that both the (2, 0)- and the (3, 0)-modes could occur, and from the frequency of every mode occurring in the experiment, it appears that the (2, 0)-mode tends to occur more often, compared with the (3, 0)-mode, and the other modes cannot occur. This is consistent with the theoretical result.

Figure 9(a) shows the experimental result for the case in which two dynamic absorbers with mass $m_1=m_2=2g$ ($\nu=1.46\times10^{-3}$) for the (2, 0)-mode were installed at an angle of 45°. Here, the (2, 0)-mode was perfectly quenched, and the envelope waveforms for the case in which the (3, 0)-mode occurred are indicated. Though the (2, 0)-mode tends to occur more often compared with the (3, 0)-mode, in this state, the (2, 0)-mode was perfectly quenched, and this mode did not occur at all. Figure 9(b) shows the experimental result for the case in which two dynamic absorbers with mass $m_1=m_2=2g$ for the (3, 0)-mode were installed at an angle of 30°. The (3, 0)-mode was perfectly quenched, and only the (2, 0)-mode occurred. Both waveforms were accompanied by beats due to the imperfection due to the dynamic absorbers. The results of the frequency analysis are shown in Figs. 9(c) and 9(d), respectively.

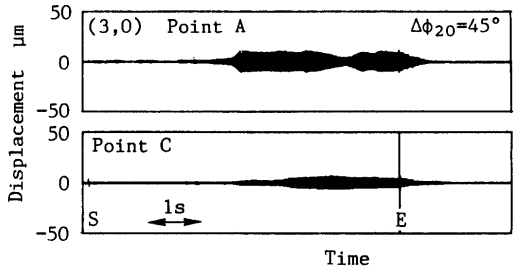

(a) Occurrence of the (3, 0)-mode when dynamic absorbers for the (2, 0)-mode were installed

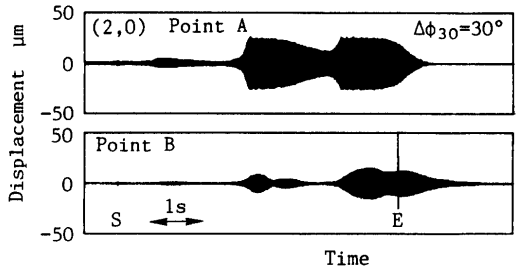

(b) Occurrence of the (2, 0)-mode when dynamic absorbers for the (3, 0)-mode were installed

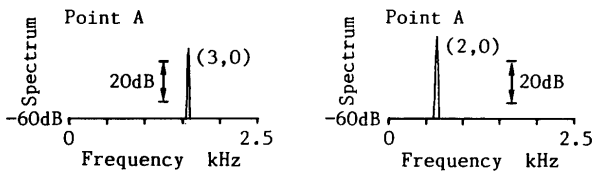

(c) Frequency analysis (d) Frequency analysis

Fig. 9 Vibration of disk with two dynamic absorbers for each mode

Figure 10 shows the envelope waveforms for the case in which a dynamic absorber with mass $m_1=15g$ ($\nu=5.46\times10^{-3}$) for the (2, 0)-mode was installed. In the first half of the time, the (2, 0)-mode occurred, and the (3, 0)-mode occurred in the latter half of the time. Because perfect quenching was impossible using one heavy dynamic absorber of 15g, it was confirmed that a few dynamic absorbers arranged at a certain angle relative to the vibration mode to be controlled are the most effective.

First, two dynamic absorbers of mass $m_1=m_2=2g$ for the (3, 0)-mode are installed at an angle of $\Delta\phi_{30}=30°$. Then, two dynamic absorbers of mass $m_3=m_4=2g$ for the (2, 0)-mode are installed. Figure 11 shows the envelope waveforms at point A when the opening angle $\Delta\phi_{20}$ is changed under the condition mentioned above. In Fig. 11, the arrangements of the

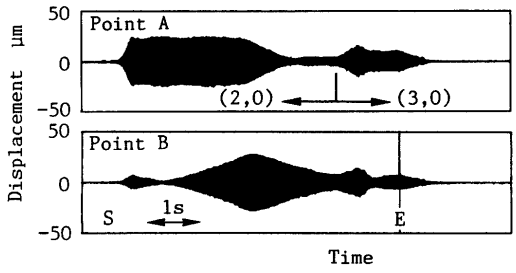

Fig. 10 Example of envelope waveforms when a dynamic absorber for the (2, 0)-mode was installed

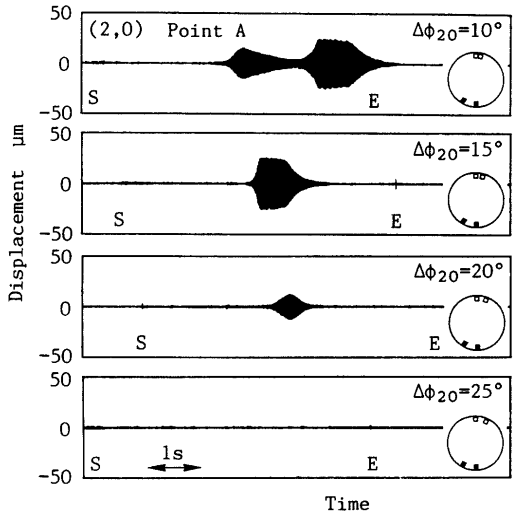

Fig. 11 Effect of opening angle between dynamic absorbers for the (2, 0)-mode

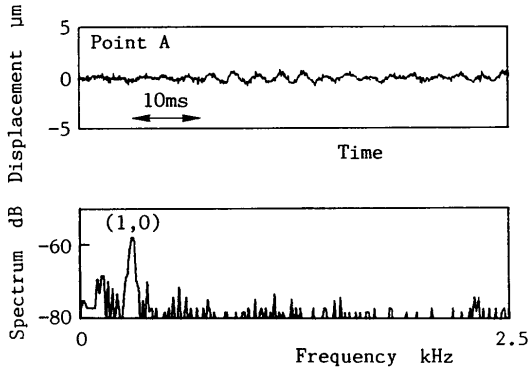

Fig. 12 Example of perfect quenching by dynamic absorbers for both the (2, 0)- and the (3, 0)-modes

dynamic absorbers are indicated in the same manner as in Fig. 5. Because of the dynamic absorbers for the (3, 0)-mode, the (3, 0)-mode does not occur at all, and so the waveforms in Fig. 11 are all those of the (2, 0)-mode. Though squeal of the (2, 0)-mode occurred up to $\Delta\phi_{20}=20°$, the (2, 0)-mode was perfectly quenched at the angle of 25°.

Figure 12 shows the resulting waveform at point A and the result of the frequency analysis for the case in which two dynamic absorbers for the (3, 0)-mode and two for the (2, 0)-mode are simultaneously installed at the opening angles of 30° and 45°, respectively. The very small vibration shown in Fig. 12 corresponds to that of the (1, 0)-mode. Because both the (2, 0)- and the (3, 0)-modes are perfectly quenched, the (1, 0)-mode occurs. However, the vibration is at the noise level, that is, very weak, and intermittent and so in practice, a state was realized in which squeal does not occur at all. From the finding that the squeal is perfectly quenched at an angle of $\Delta\phi_{20}\geqq 25°$, the experimental result agrees well with the numerical computational one because the quenching effect is increased as the opening angle reaches 45° according to the numerical computational result. Then, we observed the vibrations of the dynamic absorbers when only the rotating speed of the circular plate was set to zero in this state. As a result, there are almost no vibrations of the dynamic absorbers, and the mode to be controlled is perfectly quenched at the initial stage of the self-excited vibration. In this respect, the behavior of the dynamic absorber for quenching the self-excited vibration is much different from that for controlling the forced vibration in which the dynamic absorber vibrates heavily to suppress the vibration.

5. Conclusions

The authors presented an approach to control perfectly the frictional vibrations generated in a rotating circular plate without the effect of internal resonances, and performed analysis and experiments. The results are summarized as follows.

(1) In order to quench the self-excited vibrations of the rotating disk by using dynamic absorbers, it is effective to arrange two dynamic absorbers at an angle corresponding to the interval between loop and node of the mode to be controlled. Moreover, the maximum vibration control effect is attained when the natural frequency of dynamic absorbers coincides with that of the mode to be controlled.

(2) By arranging the dynamic absorbers for all possible occurring modes according to the approach mentioned above, the self-excited vibrations are perfectly quenched.

(3) Qualitative agreement between analytical and experimental results with respect to the perfect quenching of the self-excited vibration was confirmed.

References

(1) Sueoka, A., Yoshitake, Y. and Tamura, H., Self-excited Vibrations of a Rotating Circular Plate (3rd Report, Effect of Imperfections of a Circular Plate without Internal Resonances), Trans. Jpn. Soc. Mech. Eng., (in Japanese), Vol. 55, No. 514, C (1989), p. 1330.

(2) Yoshitake, Y. and Sueoka, A., Frictional Vibrations of a Rotating Circular Plate with Imperfections (The Case of a Circular Plate with an Internal Resonance), Trans. Jpn. Soc. Mech. Eng., (in Japanese), Vol. 57, No. 533, C (1991), p. 42.

(3) Harada, H., Okamura, H., Nishiwaki, M. and Ikeuchi, T., Study on Brake Noise (2nd Report, On Disk Brake Squeal), Trans. Jpn. Soc. Mech. Eng., (in Japanese), Vol. 55, No. 512, C (1989), p. 932.

(4) Zhang, W., Matsuhisa, H., Honda, Y. and Sato, S., The Vibration Reduction of a Railway Wheel by Cantilever-Type Dynamic Absorbers (2nd Report, Optimal Tuning of Absorbers and Experiment), Trans. Jpn. Soc. Mech. Eng., (in Japanese), Vol. 54, No. 508, C (1988), p. 2942.

(5) Sueoka, A., Ayabe, T., Kurahachi, T. and Ohishi, K., Vibration Control of a Rotating Disk by Dynamic Absorbers, Trans. Jpn. Soc. Mech. Eng., (in Japanese), Vol. 57, No. 535, C (1991), p. 714.

(6) Sueoka, A., Yoshitake, Y., Tamura, H. and Horita, K., Self-excited Vibrations of a Disk Subjected to Frictional Forces at Two Points on Outer Circumference, Trans. Jpn. Soc. Mech. Eng., (in Japanese), Vol. 52, No. 473, C (1986), p. 16.

(7) Nayfeh, A. H. and Mook, D. T., Nonlinear Oscillations, (1979), p. 56, John Wiley & Sons.

(8) Sueoka, A., Yoshitake, Y., Ryu, T., Ayabe, T. and Tamura, H., Self-Excited Vibrations of a Rotating Circular Plate (1st Report, The Case of a Circular Plate without Internal Resonances), Trans. Jpn. Soc. Mech. Eng., (in Japanese), Vol. 53, No. 485, C (1987), p. 21.